J Mater Sci (2010) 45:4858–4865
DOI 10.1007/s10853-010-4264-3

ULTRAFINE GRAINED MATERIALS

Microstructural studies on nanocrystalline oxide dispersion strengthened austenitic (Fe–18Cr–8Ni–2W–0.25Y_2O_3) alloy synthesized by high energy ball milling and vacuum hot pressing

P. Susila · D. Sturm · M. Heilmaier · B. S. Murty · V. Subramanya Sarma

Received: 18 November 2009 / Accepted: 22 January 2010 / Published online: 6 February 2010

Abstract In the present work, nanostructured (Fe–18Cr–8Ni–2W) austenitic base and oxide dispersion strengthened (ODS) alloy powders were produced through mechanical alloying and these nano powders were consolidated by vacuum hot pressing. The results showed that initially bcc solid solution formed in both the alloys and this transformed to fcc with continued milling. The bcc solid solution formation and the subsequent transformation to fcc were significantly faster in the ODS alloys when compared to the base alloy. In the ODS alloy, a grain size of ~25 nm is achieved within 5 h of milling. Study of variation of microhardness of mechanically alloyed powder particles with grain size showed linear Hall–Petch kind of behavior. Following vacuum hot pressing of mechanically alloyed powders, nearly fully dense (>99% of theoretical density) compacts were obtained with a grain size of ~80 nm. The bulk hardness of base and ODS alloys are ~530 and ~900 HV, respectively. These are significantly higher than the values reported in the literature so far. The enhanced strength the ODS alloy is due to increased dislocation density and presence of fine dispersoids along with the nanocrystalline grains.

P. Susila · B. S. Murty · V. Subramanya Sarma (✉)
Department of Metallurgical and Materials Engineering, Indian Institute of Technology Madras, Chennai 600036, India
e-mail: vsarma@iitm.ac.in

D. Sturm
Institute for Materials and Joining Technology, Otto-von-Guericke University Magdeburg, 39104 Magdeburg, Germany

M. Heilmaier
Department of Materials Science, TU Darmstadt, 64287 Darmstadt, Germany

V. Subramanya Sarma
Department of Materials Science and Engineering, North Carolina State University, Raleigh 27695, USA

Introduction

Materials for future power plants require enhanced creep resistance, corrosion resistance, and oxidation resistance. Use of conventional steels is limited up to 500 °C due to recrystallization, grain coarsening, and precipitate dissolution that result in reduced creep resistance above these temperatures [1]. Ferritic–martensitc steels [2] are widely used in nuclear power plants due to their excellent void swelling resistance, but the creep resistance is poor due to their open bcc structure. Austenitic steels and Ni base alloys have much better creep resistance due to their close packed structure and as Ni base alloys are prohibitively expensive, austenitic steels have good potential. Conventional austenitic stainless steels (ASS) have good corrosion resistance and high temperature mechanical properties. The creep properties of the ASS can be further enhanced through oxide dispersion strengthening (ODS), in which fine particulate material, usually metallic oxide particles (which are stable up to very high temperatures) is dispersed. These ultrafine oxide particles (usually Y_2O_3) will retard the recrystallization, grain coarsening, and grain boundary sliding thereby significantly improving the creep strength [3–5]. This approach is well established and considerable knowledge base exists in processing, microstructure and creep properties in case of ferritic steels and Ni base alloys [6, 7]. ODS alloys produced through conventional casting processes usually have non-uniform distribution of dispersoids. Mechanical alloying (MA) is a powder processing route by which uniform distribution of oxide particles can be achieved throughout the matrix. MA has been used to

produce nanocrystalline materials, equilibrium and non-equilibrium materials. High energy ball milling/MA is considered to be a better technique to synthesize large quantities of nanostructured materials [8]. However, there is limited knowledge base on austenitic ODS alloys by MA.

Studies on MA of Fe–Ni system showed that the concentration ranges for the formation of BCC and FCC single phase solid solutions depend on milling intensity and shift to lower Ni concentrations with increasing milling energy [9, 10]. It was also reported that annealing of MA Fe–Ni powders resulted in the extension of the concentration range for FCC solid solution [9]. Studies on the effect of milling speed in Fe–45% Ni alloy revealed that higher kinetic energy leads to an increase in lattice parameter and a decrease in grain size [11]. Enayati and Bafandeh have studied typical ASS compositions, i.e., Fe–18Cr–8Ni, Fe–15Cr–15Ni, and Fe–15Cr–25Ni by MA and reported that bcc solid solution is obtained in alloys with 8 and 15% Ni and an fcc solid solution is obtained with 25% Ni [12]. They also reported that the bcc solid solution is relatively stable even after annealing the MA powder at 700 °C for 1 h [12]. The phases obtained by MA were not consistent with those expected from equilibrium phase diagram. Recently Phaniraj et al. [13] studied Y_2O_3 dispersed Fe–20Ni–14Cr–2.5Mo–2.5Al–2Mn ODS alloy prepared by MA and reported that alloying took place after 2 h of milling and a single phase fcc solid solution is formed within 8 h of milling. The above studies indicate that phase formation in MA is strongly sensitive not only to the milling parameters/conditions, but also to the composition. The addition of Y_2O_3 appears to accelerate the alloy formation [13]. In the present study, microstructure, phase formation and hardness of Fe–18Cr–8Ni–2W base alloy and Fe–18Cr–8Ni–2W–$0.25Y_2O_3$ ODS alloy prepared by MA were reported. The microstructure and hardness of consolidated MA powders (by vacuum hot pressing) is also presented. The different contributions to the overall room temperature strength are assessed and compared with the experimental results.

Experimental procedure

The nominal compositions of the alloys studied in this work are (by wt%) Fe–18Cr–8Ni–2W and Fe–18Cr–8Ni–2W–$0.25Y_2O_3$. Elemental powders of Fe, Cr, Ni, and W with <45 μm particle size and >99.5% purity were used for MA. Elemental powders of Fe, Cr, Ni, W, and nanostructured Y_2O_3 (pre-ball milled) were mechanically alloyed at room temperature in Fritsch Pulversitte-5 planetary mill with WC vial and 10-mm diameter WC balls. Milling was carried out at 300 rpm with a ball-to-powder ratio of 10:1 in toluene medium which serves as a process control agent (PCA). Milled powders were characterized by X-ray diffraction (XRD) technique using a Shimadzu X-ray diffractometer with Fe Kα (λ is 0.193604 nm) radiation for crystal structure determination, crystallite size, and lattice strain calculations. Powders were mounted on a resin and metallographically polished to observe the microstructure of individual powder particles in as-milled condition and for evaluating the microhardness of powders using a MHT-10 microhardness tester with a load of 5 g and dwell time of 10 s. An average value from 15 indentations made on the powder samples is reported. The powders were vacuum hot pressed (P O Weber Hot press Germany) with a pressure of 200 MPa at 900 °C under a vacuum of 10^{-3} mbar. Bulk Vickers hardness (HV_{10}) was measured on consolidated samples by using Otto-Wolpert-Werke hardness tester with a load of 10 kg and a dwell time of 15–20 s. Transmission electron microscopy (TEM) studies were carried out on a Phillips CM20 operated at 200 kV. Samples for TEM studies on consolidated specimens were prepared by dimpling (Gatan Model 656) followed by ion milling (Gatan Model 691).

Results and discussion

Microstructure and mechanical properties

Figure 1a, b shows the XRD patterns of Fe–18Cr–8Ni–2W and Fe–18Cr–8Ni–2W–$0.25Y_2O_3$ powders milled for different milling times. The extent of alloying and evolution of phases can be observed from XRD patterns. In XRD pattern of pre-milled powder (0 h) individual elemental peaks of Fe, Cr, Ni, and W were observed (Fig. 1a). In case of base alloy, solid solution formation (corresponding to disappearance of peaks of most of the major alloying elements) was observed after 15 h of milling (Fig. 1a). However, the solid solution formed after 15 h of milling is bcc and the transformation to fcc begins after 20 h of milling. The transformation does not seem to be complete even after 25 h of milling implying a mixture of bcc and fcc phases is present after 25 h of milling. This is seen from the slow scan XRD pattern of 25 h milled powder (Fig. 1b). In the ODS alloy, formation of solid solution occurred within 5 h of ball milling and the structure is also bcc (Fig. 1c). Here, the transformation to fcc begins earlier, i.e., after 10 h of milling. Unlike in the case of the base alloy, the bcc–fcc transformation is more or less complete (though a very small fraction of bcc phase could still be present) after 20 h of milling as seen from the slow scan XRD pattern (Fig. 1d). The acceleration of solid solution formation in the ODS alloy is attributed to the presence of yttria (though present in very small quantity) which due to its hard and brittle nature is expected to accelerate the work hardening and fracture. Phaniraj et al. [13] also reported a

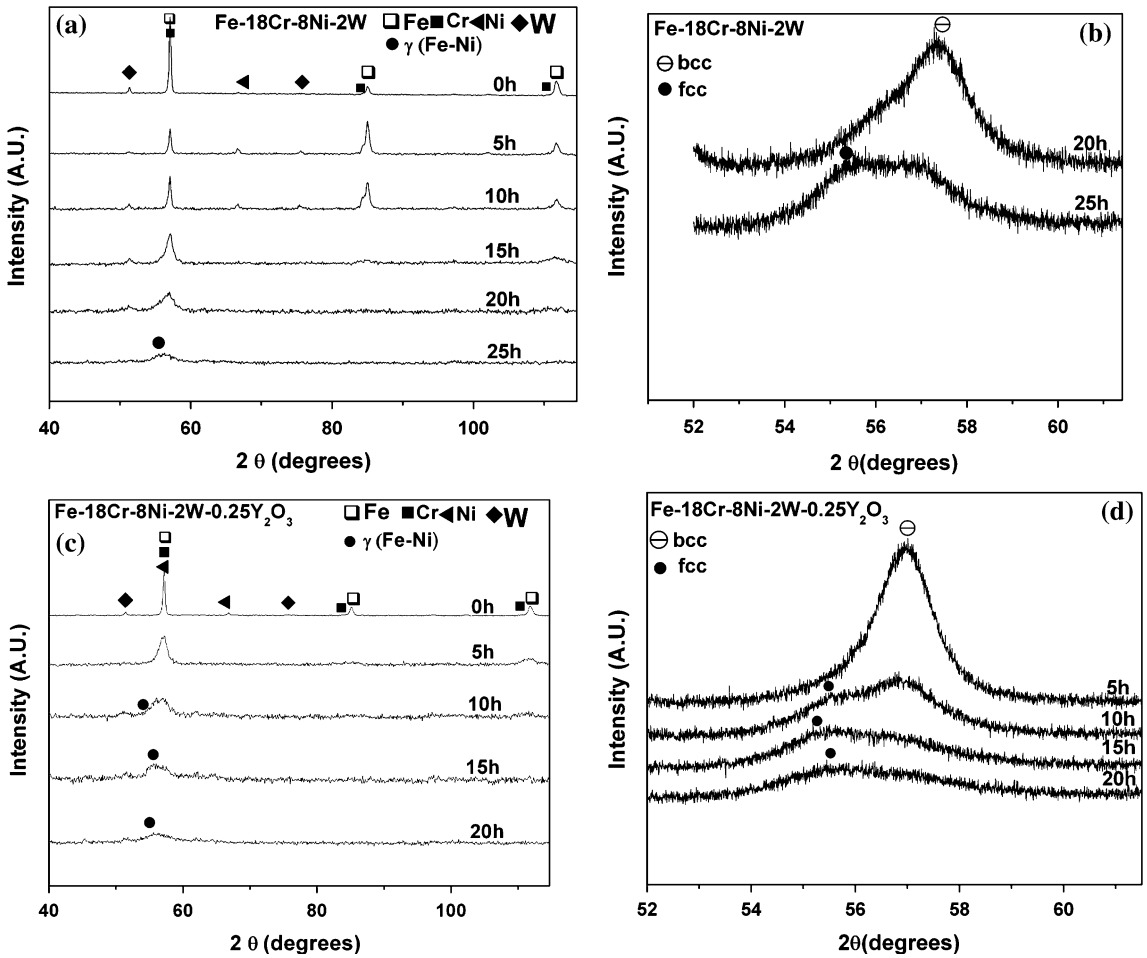

Fig. 1 X-ray diffraction patterns from milled powders of (**a**) Fe–18Cr–8Ni–2W (base alloy), (**b**) high resolution scan for base alloy in (**a**), (**c**) Fe–18Cr–8Ni–2W–0.25Y_2O_3 (ODS alloy), and (**d**) high resolution scan for ODS alloy in (**c**)

similar result. However, formation of austenitic (fcc) solid solution in the work of Phaniraj et al. [13] was also due to the higher Ni content and additionally due to the presence of Mn, both of which are strong austenite stabilizers. However, in the present work, austenite (fcc) phase formation was observed with a lower amount of Ni. This is in contrast to the results reported by Enayati and Bafandeh [12], who found the formation of a bcc solid solution in Fe–18Cr–8Ni alloy even after 60 h of milling. This is likely due to the lower milling intensities (steel balls with steels vials were used by Enayati and Bafandeh [12]) employed. In the present study, WC vial and balls are used and these impart much higher energy to the powders during milling. Further, the ball-to-powder ratio in our study was higher (10:1) as compared to 6:1 used by Enayati and Bafandeh [12]. Du et al. also reported that the formation of final solid solution depends on the composition of alloy [14]. In the present investigation, addition of 2% W (W is a ferrite stabilizer) to the regular austenitic base composition equivalent to AISI 304 grade (Fe–18Cr–8Ni), has not altered the stability of fcc phase. This is crucial because W is an important alloying addition which is expected to enhance the high temperature strength and creep resistance and retention of fcc structure is also critical for reasons discussed above.

Figure 2a, b shows the variation of crystallite size (obtained from XRD peak broadening) with milling time in both the alloys, i.e., base alloy and ODS alloy. The crystallite size and lattice strain in milled powders were calculated from (110) peak for bcc phase and (111) peak for fcc phase by using Voigt function [15]. The instrumental broadening was determined by using standard Fe sample and this was subtracted from the data before the above calculations. The Cauchy and Gaussian functions were obtained from the full width at half maximum (FWHM), peak positions and the integral breadths. Figure 2 shows that crystallite size decreases with increasing milling time in both the alloys. However, the rate of decrease is significantly enhanced with the addition of yttria and after 5 h of milling a crystallite size of 25 nm is achieved in the ODS alloy. This is also consistent with the above results on acceleration of solid solution formation in the ODS alloy.

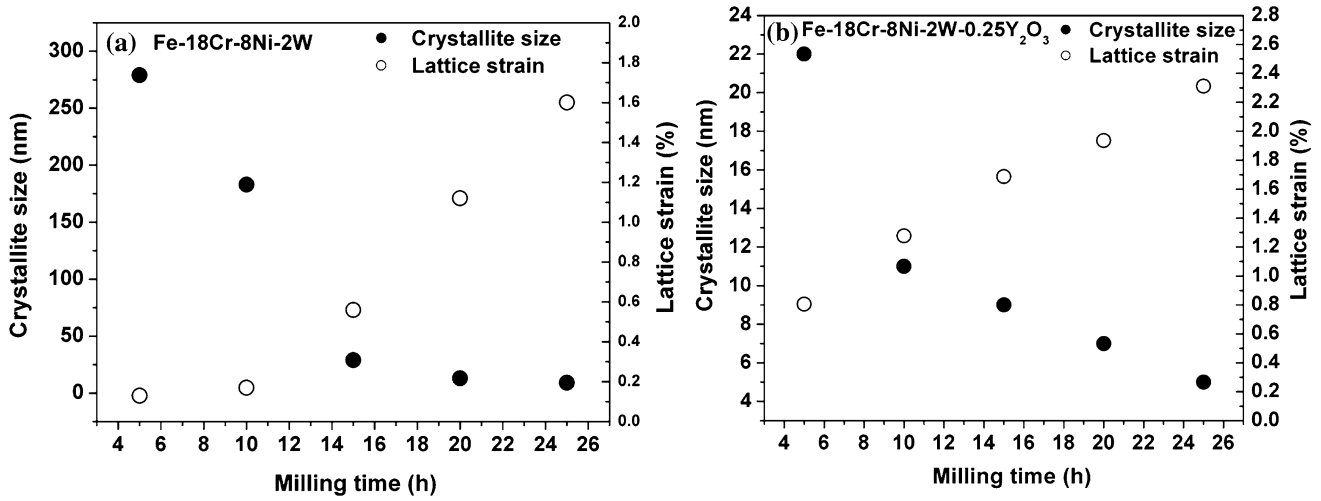

Fig. 2 Variation of crystallite size and lattice strain with milling time in (**a**) Fe–18Cr–8Ni–2W and (**b**) Fe–18Cr–8Ni–2W–0.25Y_2O_3 alloys

The lattice strain of the ODS alloy powders is also significantly higher and ~2.3% in ODS alloy compared to about 1.6% in the base alloy (Fig. 2). The increased lattice strain is due to the large number of defects produced in milling/MA of ODS alloy.

Lattice parameters (LP) of bcc and fcc solid solutions were calculated from Fe (110) and (111) peaks using Bragg's law. The lattice parameter of bcc Fe (110) was 0.2858 nm and it increased with milling time. This can be attributed to the solid solution formation and alloying. There are no significant differences in the LP of base alloy and ODS alloy. The lattice parameters of fcc phases are 0.35381 and 0.3549 nm after 25 and 15 h of milling in base alloy and ODS alloy, respectively (Fig. 3). Gheisari et al. studied the lattice parameter in Fe–45Ni alloy and reported that the lattice parameter increased with increase in milling intensity and stabilized at a value of around 0.359 nm [11]. The TEM micrograph and selected area diffraction pattern from 25 h milled powders of the ODS alloy Fe–18Cr–8Ni–2W–0.25Y_2O_3 are shown in Fig. 4a,

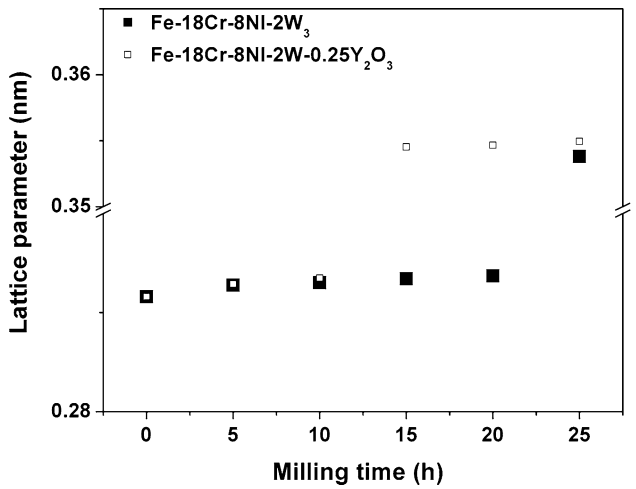

Fig. 3 Variation of lattice parameter with milling time in Fe–18Cr–8Ni–2W and Fe–18Cr–8Ni–2W–0.25Y_2O_3 alloys

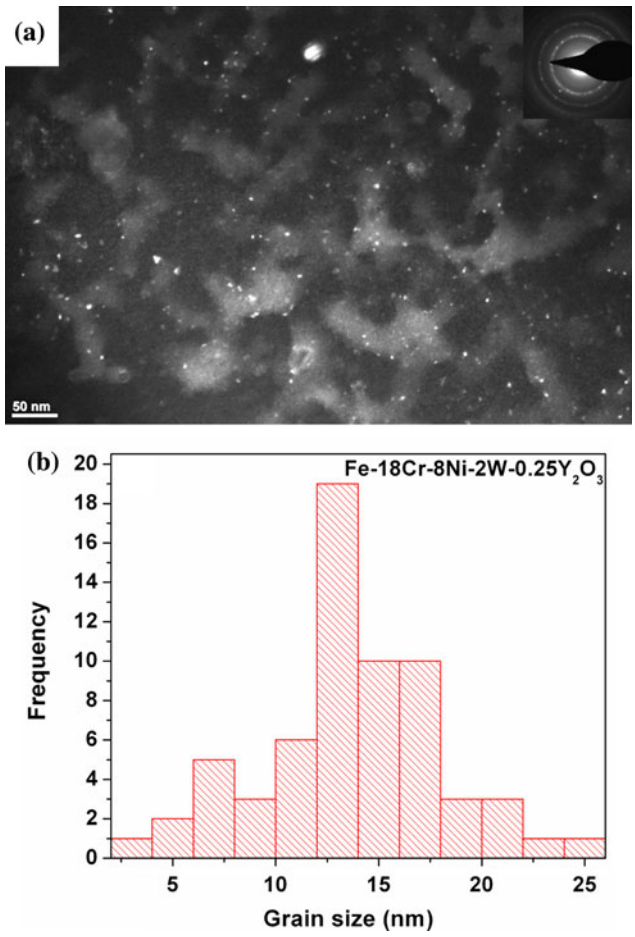

Fig. 4 (**a**) Dark field image of milled (for 25 h) powders of ODS alloy Fe–18Cr–8Ni–2W–0.25Y_2O_3 (inset shows corresponding SAD pattern) and (**b**) grain size distribution

which confirm that the grain size is in the nanometer range. Analysis of grain size distribution (Fig. 4b) revealed that the average grain size is 13 ± 4 nm.

Figure 5 shows the variation of microhardness values of the milled powders of base and ODS alloys as a function of $d^{-1/2}$ (Hall–Petch type of plot), where "d" is the grain/crystallite size. The plot is linear up to a crystallite size of 5 nm indicating that grain boundaries to be the major obstacles to dislocations. The open symbols in Fig. 5 show the HV_{10} of base and ODS alloys. It is clear that the ODS alloy has a significantly higher strength/hardness when compared to the base alloy. The contribution to strength from different strengthening mechanisms is discussed in the following section.

Consolidation of the MA powders by hot pressing in vacuum at 900 °C has resulted in ~99 and 99.5% of the theoretical density (~7.9 g/cc for AISI 304) for ODS and base alloys, respectively. The composition of the alloys on consolidated samples was measured by SEM–EDAX and is given in Table 1. Yttria content is estimated from yttrium percentage obtained from EDAX area analysis. It can be seen that the composition is quite close to the nominal composition. Figure 6a–c shows TEM micrographs from the hot pressed base alloy. The ring pattern of SAD indicates that even after consolidation at a temperature of 900 °C, the grain size is in the nanocrystalline regime. Linear intercept method was used to determine the grain size from TEM images using the relation, $\bar{d} = F_S F_d \bar{l}$, where $\bar{d}$ is the average grain size, F_S is a shape factor (taken as 1.5 assuming spherical grains), F_d is the distribution factor (taken as 1 for uniform distribution) and $\bar{l}$ is the average intercept length [16]. The microstructure consists of equiaxed grains (40–200 nm) and the grain size distribution is shown in Fig. 6b. The average grain size was found to be ~130 ± 33 nm. A dark field image is shown in Fig. 6c. It is well known that fcc metals and alloys with low stacking fault energy form annealing or growth twins following cold working and annealing. Figure 6d shows very fine annealing twins and these are due to severe cold working (during ball milling) and subsequent annealing during hot pressing. Figure 7 shows the TEM micrographs of the consolidated ODS alloy and the grains in ODS alloy are also equiaxed and nanocrystalline (Fig. 7a). This is also confirmed by the SAD pattern (inset in Fig. 7a). Analysis of grain size distribution (Fig. 7b) indicates that the average grain size is 110 ± 34 nm. This is only slightly lower than that obtained in the base alloy. The yttria particles visible in Fig. 7c, d are spherical in shape and are ~20–30 nm in diameter. They contribute significantly to the strengthening as can be seen from the fact that the macrohardness of hot pressed Fe–18Cr–8Ni–2W and Fe–18Cr–8Ni–2W–0.25Y_2O_3 alloys are 527 HV_{10} and 894 HV_{10}, respectively. Fujiwara and Ameyama [17] studied the hardness of nanocrystalline austenitic-ferritic alloy (which was prepared by mechanical milling and hot pressing of 316L alloy powder) and reported a value of 306 HV at a grain size of ~620 nm. It is obvious that much finer grain size achieved in the present study contributed to increased strength/hardness. Figure 7e shows the enlarged SAD pattern from ODS alloy and it confirms the fcc matrix and (222) reflection from yttria particles is also seen.

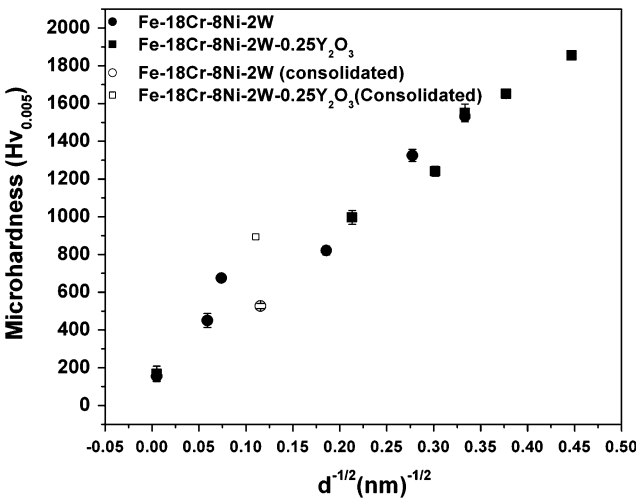

Fig. 5 Hall–Petch type plot showing variation of microhardness with $d^{-1/2}$ for in Fe–18Cr–8Ni–2W and Fe–18Cr–8Ni–2W–0.25Y_2O_3 alloys

Table 1 Chemical composition of the alloys (wt%) alloys

Elements	Fe	Cr	Ni	W	Y_2O_3
Base material	73.37	17.12	7.19	2.32	–
ODS alloy	72.54	17.34	7.67	2.2	0.25[a]

[a] Estimated from Y content with assumption that Y exists as Y_2O_3

Correlation between microstructure and mechanical properties

In this section, the contributions to the overall strength (at room temperature) from the different strengthening mechanisms were calculated for the base and ODS alloys and compared with the experimental results. The experimental strength at room temperature was obtained from hardness measurements through the relationship, $\sigma_y = 1/3$ HV. The different strengthening mechanisms are (a) solid solution strengthening (σ_{ss}), (b) dislocation strengthening (σ_{dis}), (c) grain size strengthening (σ_{gs}), and (d) dispersion strengthening (σ_{dp}) [18, 19]. Assuming a linear additive relation gives

$$\sigma_y = \sigma_{ss} + \sigma_{gs} + \sigma_{dis} + \sigma_{dp} \quad (1)$$

In the base alloy, the contributions to yield strength come from σ_{ss}, σ_{gs}, and σ_{dis} and in the ODS alloy there is an additional contribution from σ_{dp}.

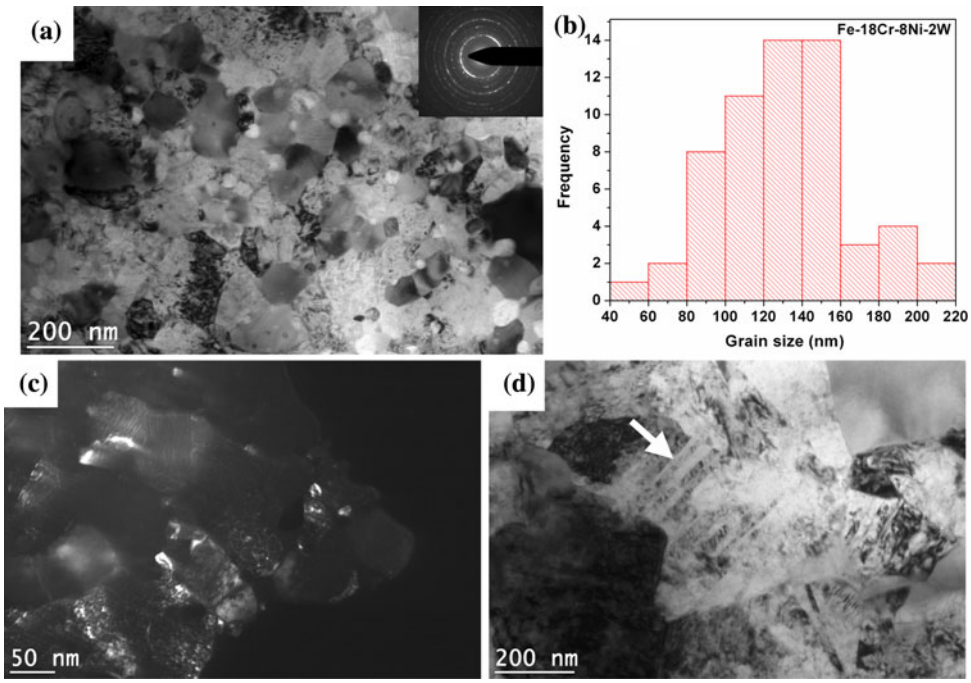

Fig. 6 TEM micrographs of vacuum hot pressed Fe–18Cr–8Ni–2W alloy (**a**) bright field image showing nanocrystalline grains (inset shows corresponding SAD pattern), (**b**) grain size distribution, (**c**) dark field image of the same alloy, and (**d**) bright field image showing nanotwins in this alloy

Solid solution strengthening

The solid solution strengthening is due to the interstitial and substitutional elements present in that particular alloy system. In the alloy system under study, the major alloying elements are Cr, Ni, and W and these form a substitutional solid solution. However, the presence of small amounts of interstitial elements, i.e., C, N, and O (due to contamination during ball milling) could not be ruled out. However, this is neglected in the present calculation. The strengthening due to substitutional elements is given by following expression for Fe [20, 21]

$$\sigma_{ss} \approx 0.00689 K X^{n}, \tag{2}$$

where "K" is strengthening coefficient (K values for Cr, Ni, and W is 1,400, 6,100, and 11,000 respectively) [20, 21], "X" is the nominal concentration of elements (in at.%) present in the alloy, "n" is constant and equal to 0.75 [20]. The factor 0.00689 is for converting value from psi (pound per square inch) to MPa [21]. From Eq. 2, the contribution from solid solution strengthening due to substitutional elements for Fe–18Cr–8Ni–2W and for Fe–18Cr–8Ni–2W–0.25Y_2O_3 is found to be ~330 MPa.

Grain size strengthening

The strengthening due to grain refinement is often accounted through a Hall–Petch type relation.

$$\sigma_{gs} \approx \sigma_0 + k d^{-1/2}, \tag{3}$$

where "σ_0" is friction stress and is taken 30 MPa (for pure Fe), "k" is constant and is taken as 0.274 $MNm^{-3/2}$ (a reported value for ultra fine grained ASS [22]) "d" is grain size (m). The average grain size measured from TEM micrographs was 131 nm for Fe–18Cr–8Ni–2W base alloy and 113 nm for Fe–18Cr–8Ni–2W–0.25Y_2O_3 ODS alloy. With the above parameters, the contribution to yield strength from grain size strengthening is 787 and 835 MPa for base and ODS alloys, respectively.

Dislocation strengthening

The increase in strength due to the dislocation density is given by the following equation [23]:

$$\sigma_{dis} = \alpha M G b \sqrt{\rho}, \tag{4}$$

where "α" is a constant (0.25–1), "G" is shear modulus (83 GPa for Fe), "b" is burgers vector (0.251 nm), "M" is Taylor's factor (~3 for randomly oriented fcc polycrystals), and "ρ" is the dislocation density (per m^2). The dislocation density "ρ" in the consolidated base and ODS alloys was calculated by the following equation:

$$\rho = \frac{2\sqrt{3}\langle \varepsilon^2 \rangle^{1/2}}{Db}, \tag{5}$$

where "ε" is the average microstrain (the average microstrain for base and ODS alloy are 0.157 and 0.26%, respectively) and "D" is the average crystallite size obtained from XRD analysis (87 and 78 nm for base and ODS alloys, respectively), "b" is Burgers vector (nm). The

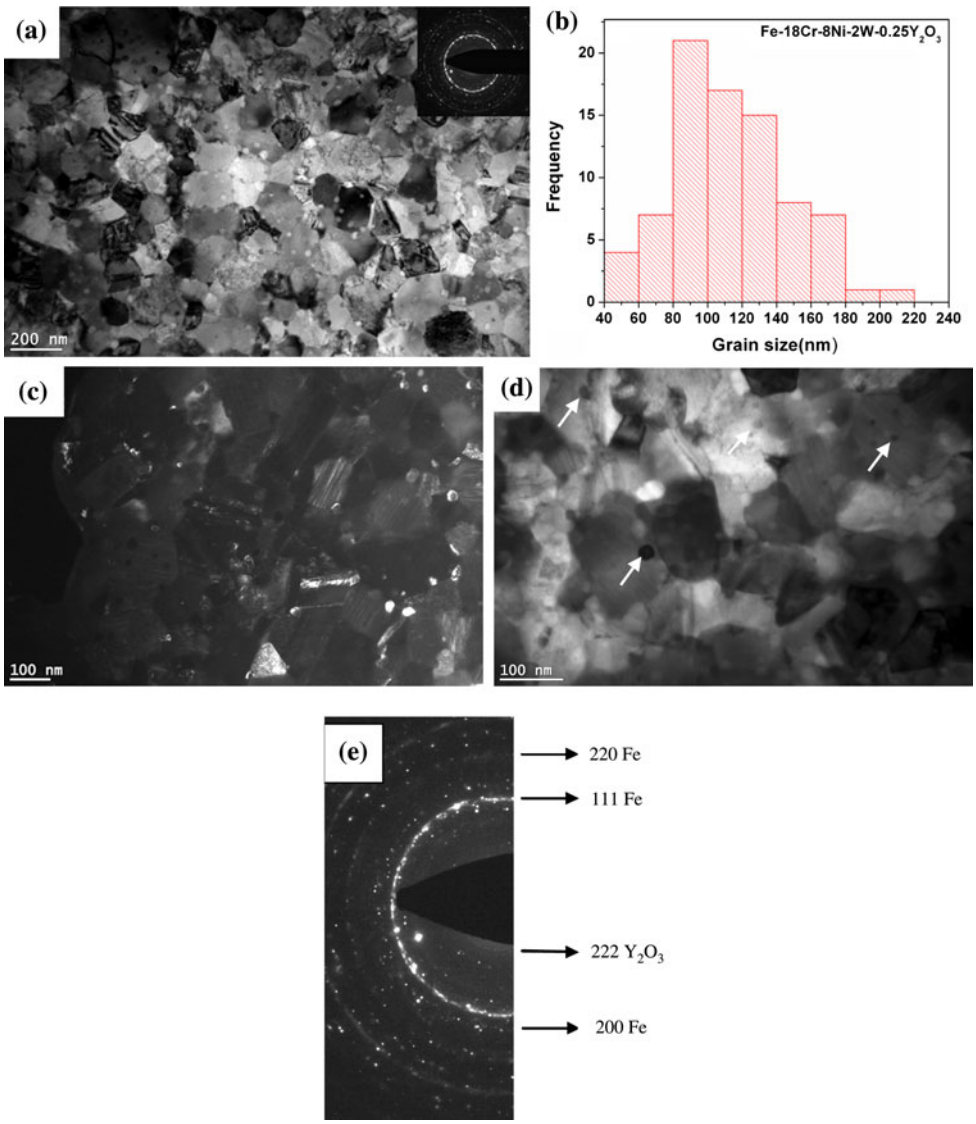

Fig. 7 TEM micrographs of vacuum hot pressed Fe–18Cr–8Ni–2W–0.25Y_2O_3 ODS alloy. (**a**) Bright field image showing nanocrystalline grains and nanotwins (inset shows corresponding SAD pattern), (**b**) grain size distribution, (**c**) dark field image showing dispersoids and nanotwins, (**d**) bright field at higher magnification showing dispersoids, and (**e**) SAD pattern shown in inset (**a**) is enlarged and indexed

dislocation densities were found to be $\sim 2.5 \times 10^{14}$ and $\sim 4.8 \times 10^{14}$ m^{-2} for base ODS alloys, respectively. From Eq. 4, the strength contribution due to dislocation density is estimated for a range of α values (from 0.25 to 1) and these are given in Table 2.

Dispersion strengthening

The contribution to strength from dispersion strengthening was estimated by the following equation [24]:

$$\sigma_{dp} = \frac{MGb}{L - 2r}, \quad (6)$$

where "L" is the inter-particle spacing (180 nm was estimated from TEM micrographs using Eq. 7) and "r" is

Table 2 Calculated and experimental yield strengths of hot pressed base and ODS alloy

Strengthening mechanism (MPa)	Base alloy	ODS alloy
Solid solution (σ_{ss}) (Eq. 2)	322	330
Grain refinement (σ_y) (Eq. 3)	787	835
Dispersoids (σ_{dp}) (Eq. 6)	–	347
Dislocations (σ_{dis})		
$\alpha = 0.25$ in Eq. 4	247	343
$\alpha = 0.5$ in Eq. 4	494	685
$\alpha = 1$ in Eq. 4	988	1,370
Total (calculated) ($\alpha = 0.25$ in Eq. 4)	1,356	1,855
Total (calculated) ($\alpha = 0.5$ in Eq. 4)	1,603	2,197
Total (calculated) ($\alpha = 1$ in Eq. 4)	2,097	2,882
Experimental yield strength (1/3 HV)	1,724	2,924

the average radius of the particle size (13 ± 4 nm). The volume fraction (f) of yttria estimated from rule of mixtures was 0.0039 and the inter-particle spacing is given in terms of average particle radius and the volume fraction as [25].

$$L \approx \frac{r}{\sqrt{f}} \tag{7}$$

The contribution of σ_{dp} toward strength of ODS alloy was estimated using Eq. 6 as 347 MPa.

The contributions to the strength from different strengthening mechanisms in the ODS alloy are listed in Table 2. It can be seen that there is a reasonable agreement between the calculated and experimental yield strength with the $\alpha \sim 0.5$ for base alloy and $\alpha \sim 1$ for the ODS alloy. This may indicate that the arrangement of dislocations is different in base and ODS alloys.

Conclusions

Nanocrystalline austenitic (Fe–18Cr–8Ni–2W) base and (Fe–18Cr–8Ni–2W–0.25Y_2O_3) ODS alloys were synthesized by MA. Accelerated reduction of crystallite size and solid solution formation were observed in ODS alloy due to presence of nano yttria particles. During MA, first a bcc solid solution was observed and with continued milling this transformed to fcc solid solution. The hardness of MA powders were found to follow Hall–Petch relation (linear dependence with $d^{-0.5}$, where "d" is the grain size) up to about 5 nm. After vacuum hot pressing of MA powders at 900 °C, the grain size is ~130 and 110 nm in base alloy and ODS alloy, respectively, and the bulk hardness is 530 and 900 HV, respectively. Evaluation of contributions from different strengthening mechanisms clearly showed that the grain refinement and dislocation strengthening are the dominant strengthening mechanisms.

Acknowledgements The authors are thankful to the DST-DAAD for the financial support (DST-DAAD Project No. INT/DAAD/P-172/2007). One of the authors (VSS) acknowledges the financial support of Indo-US Science and Technology Forum (IUSSTF) through a research fellowship.

References

1. Klueh RL, Ehrlich K, Abe F (1992) J Nucl Mater 191–194:116
2. Ukai S, Harada M, Nomura S, Shikakura S (1992) In: International symposium material chemistry in nuclear environment, Tsukuba, Japan, p 347
3. Alamo A, Lambard V, Averty X, Mathon MH (2004) J Nucl Mater 329–333:333
4. Kazimierzak B, Prignon JM, Fromont RI (1992) Mater Des 13(2):67
5. Arzt E, Behr R, Gohring E, Grahle P, Mason RP (1997) Mater Sci Eng A 234–236:22
6. Estrin Y, Heilmaier M, Dew G (1999) Mater Sci Eng A 272:163
7. Schneibel JH, Liu CT, Miller MK, Mills MJ, Sarosi P, Heilmaier M, Sturm D (2009) Scr Mater 61:793
8. Benjamin JS (1970) Metall Trans A 1:2943
9. Kaloshkin SD, Tcherdyntsev VV, Tomlin IA, Baldokhin YV, Shelekhov EV (2001) Physica B 299:236
10. Kuhrt C, Schultz L (1993) J Appl Phys 73:1975
11. Gheisari K, Javadpou S, Oh JT (2009) J Phys Conf Ser 153:012051
12. Enayati MH, Bafandeh MR (2008) J Alloy Compd 454:228
13. Phaniraj MP, Kim D-I, Shim J-H, Cho YW (2009) Acta Mater 57:1856
14. Du SW, Ramanujan RV (2005) J Magn Magn Mater 292:286
15. Keijser TH, Langford JI, Mittemeijer EJ, Vogels ABP (1982) J Appl Crystallogr 15:308
16. Han JH, Kim DY (1995) Acta Metall Mater 43(8):3185
17. Fujiwara H, Ameyama K (1999) Mater Sci Forum 304–306:47
18. Srinivasan D, Corderman R, Subramanian PR (2006) Mater Sci Eng A 461:211
19. Munoz-Morris MA, Garcia Oca C, Morris DG (2002) Acta Mater 50:2825
20. Lacy CE, Gensamer M (1944) Trans Am Soc Met 32:88
21. Li Q (2003) Mater Sci Eng A 361:355
22. Rajasekhara S, Ferreira PJ, Karjalainen LP, Kyrolainen A (2007) Metall Mater Trans A 38A:1202
23. Taylor GI (1934) Proc R Soc A 145:362
24. Cao B, Joshi SP, Ramesh KT (2009) Scr Mater 60:619
25. Gottstein G (2004) Physical foundations of materials science. Springer, New York